CHALMERS
UNIVERSITY OF TECHNOLOGY

Dynamic State Estimation based Transmission Line Protection Scheme: Performance Evaluation with Different Fault Types and Conditions

Electrical Power and Energy Systems 148 (2023) 108994

Contents lists available at ScienceDirect

International Journal of Electrical Power and Energy Systems

journal homepage: www.elsevier.com/locate/ijepes

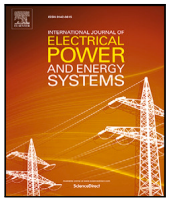

Dynamic state estimation based transmission line protection scheme: Performance evaluation with different fault types and conditions

Ankur Srivastava [a,*], Le Anh Tuan [a], David Steen [a], Ola Carlson [a], Omar Mansour [b], Dennis Bijwaard [b]

[a] Division of Electric Power Engineering, Department of Electrical Engineering, Chalmers University of Technology, Gothenburg, 41296, Sweden
[b] Smart State Technology BV, Hengelo, The Netherlands

ARTICLE INFO

Keywords:
Dynamic state estimation
Experimental validation
High impedance fault
Hidden failures
Setting-less protection
Transmission line protection

ABSTRACT

This paper presents the experimental validation of a transmission line protection scheme based on dynamic state estimation for different fault types and conditions. The protection scheme utilizes real-time high-frequency sampled measurements from advanced sensors and evaluates the operating condition of the transmission line based on which a tripping signal is generated in case a fault occurs. The validation is performed using a physical scaled-down model of a power system, consisting of a transmission line, transformer, synchronous generator, and loads. The following faults are examined during the validation: unbalanced faults under different load conditions, high impedance fault, fault current fed from both ends, hidden failure, external fault, and load change conditions. The results show that the scheme performs as intended and thus proves its efficacy to detect various types of faults. The maximum fault detection time is calculated to be 42.5 ms, while the maximum fault clearing time comes out to be 82.5 ms, on par with currently employed protection methods. The obtained results demonstrate the ability of the scheme to detect different fault types under varying conditions and avoid potential issues with relay coordination.

1. Introduction

Power system protection is one of the essential topics in power system operation which requires high accuracy, reliability, and selectivity to isolate faulted parts in case of any undesirable event. Relay mis-operations are one of the current challenges in protection, leading to interruptions in power supply and failure of existing protection schemes [1,2]. In addition, conventional transmission line protection schemes have some protection gaps and limitations: (i) Non-pilot distance and directional overcurrent schemes face issues such as complex coordination, simultaneous tripping of both ends of the line, insensitivity to high impedance faults; (ii) Pilot relaying schemes face issues such as communication failures which could lead to scheme failure, detection of high impedance; and (iii) Differential protection has limitations such as relay desensitization forced due to capacitive currents in long transmission lines, detection of high impedance faults in long transmission lines, current inversion in series compensated transmission lines that could lead to failures [3–5]. Further, the unusual fault current and voltage characteristics from inverter-interfaced renewable resources also bring challenges to conventional protection schemes [2,6].

A potential solution to address some of these protection gaps and limitations is offered by a dynamic state estimation (DSE)-based protection scheme [7]. The motivations to apply DSE in the protection applications are explained in [8]. Some of the key motivations as mentioned in [8] are (i) DSE provides real-time operating conditions and enhanced visibility of the system, (ii) DSE can accurately estimate the system's dynamic states and track the complex system dynamics which can be used for evaluating fault conditions, (iii) the application of DSE in protection could help in avoiding complex coordination issues among relays by examining the consistency between the measurements and the dynamic model of the transmission line, and, (iv) the inherent redundancy available with the measurements in DSE could help in detecting hidden failures by identifying and rejecting bad data. The idea of applying DSE in protection is further supplemented with recent advancements in measurement devices and substation automation, which can provide good quality measurements with high sampling rates. The feasibility of the DSE-based protection solution is discussed in [9]. A detailed explanation of this scheme along with its capabilities to improve zone protection, detection, and self-healing against hidden failures is presented in [3]. Further, a dynamic state

* Corresponding author.
E-mail address: ankur.srivastava@chalmers.se (A. Srivastava).

https://doi.org/10.1016/j.ijepes.2023.108994
Received 17 June 2022; Received in revised form 12 November 2022; Accepted 19 January 2023
Available online 31 January 2023

estimation-based protection scheme (DSEBPS) is a generalized concept and could be applied to power systems and their components such as series compensated transmission lines [4], transmission line fault classification [10], and distribution systems with high penetration of distributed energy resources [11], etc. A centralized substation protection scheme is developed in [12] which employs a DSE-based protection scheme. Synchrophasor-based state estimation is utilized in [13] to develop a protection scheme for a microgrid. In [14], a protection scheme for large synchronous generators during out-of-step conditions is developed based on DSE. Similarly, a novel fault location method for transmission lines in modular multilevel converter-HVDC grids is proposed in [15] which utilizes both DSE and gradient descent. In [16], a wide-area backup protection scheme is developed based on the cubature Kalman filter-based DSE which acquires full network observability with limited phasor measurement unit (PMU) measurements. Besides finding applications in the protection of various components, most of the existing studies have used simulation or hardware-in-loop (HIL) platforms to study the performance of DSEBPS, which limits the practical application of the scheme. Thus, field testing or laboratory testing of DSEBPS with physical components is required to increase the technology readiness level so that it reaches the real world faster.

Our previous work [17] has demonstrated the feasibility of using DSEBPS for transmission line protection by performing the simulations under different fault types and conditions and validation using an experimental setup, consisting of an accurate scaled-down model of a simple power system. The experimental setup also included the interface of circuit breakers, preparation of communication requirements, and the setting up of advanced sensors as an affordable and reliable real-time measurement solution. After the preparation of the experimental setup, the DSE algorithm along with the open platform of the advanced sensors was implemented in Python to be employed in carrying out the test and then evaluating the practical feasibility of DSEBPS. However, the work presented in [17] has validated the performance of DSEBPS for a three-phase fault only, while in reality transmission lines are exposed to different types of faults and conditions. From a design perspective, any new protection scheme should be able to accurately and timely detect all the different fault types and conditions. In this regard, this paper continues the work presented in [17] by additionally evaluating the performance of DSEBPS in the case of a transmission line with different fault types and conditions, such as single-line-to-ground and double-line-to-ground fault under resistive and inductive load, high impedance fault, fault current fed from both ends, hidden failure, external fault, and load change conditions. Prior to the experimental validation, this work involves the implementation and execution of DSEBPS in simulation and thereafter extensive case studies, which help to set up the requirements of the experimental setup. An open platform approach employing Python is adopted for the implementation of DSEBPS in experimental validation. The advanced sensors used in the setup provide real-time measurements which are one of the key inputs for DSEBPS. The experimental validation of DSEBPS in transmission line protection under different fault types contributes to the enhancement of the maturity of the scheme and brings it closer to real-world applications. The main contributions of the paper can be summarized as follow:

- Preparing the extended experimental setup for the validation of DSEBPS in the laboratory environment which includes setup of inductive loads, synchronization of generator with the grid, different fault impedance, etc.
- Carrying out different fault test cases for a transmission line under different fault types and conditions such as unbalanced faults under different load conditions, high impedance fault, fault current fed from both ends, hidden failure, external fault, and load change conditions.
- Evaluating performance and validating the practical feasibility of DSEBPS in the laboratory environment, which is a step ahead of the conventional simulation or HIL studies, and thus advancing the maturity (technology readiness level) of DSEBPS for transmission line protection.

The rest of the paper is organized as follows. The description of the dynamic state estimation-based protection scheme for the transmission line is given in Section 2. The details of the case study are presented in Section 3. Section 4 discusses the results obtained from different case studies. The details about the estimation error are presented in Section 5. The explanation of the fault clearing time is given in Section 6. Finally, the concluding remarks are outlined in Section 7.

2. Dynamic state estimation-based protection scheme for transmission lines

2.1. Introduction to DSEBPS: How it works?

DSEBPS has been motivated by differential protection and monitors all the physical laws that a transmission line should satisfy. The dynamic model of the transmission line is constantly observed by DSE and any abnormality in the operating conditions is comprehended. The real-time measurements from the terminals of the transmission line are provided as inputs to DSE which then estimates the current states. Subsequently, the Chi-square test is performed to evaluate the goodness of fit between the transmission line dynamic model and measurements. The results from the Chi-square test are quantified for evaluating the confidence level in transmission line health [3]. The confidence level is then interpreted to generate the trip signal to isolate the transmission line by clearing the fault. In this work, if the objective function remains above the threshold value for forty consecutive samples, then the confidence level goes low, and hence a trip signal is sent to the breakers. It shall be noted that any user-defined number of consecutive samples could be used for the trip logic.

2.2. Problem formulation

2.2.1. Dynamic modelling of transmission line

The dynamic modelling is done using the algebraic quadratic companion form (AQCF) and quadratic integration (QI) method. The three-phase representation of one π-section of a transmission line with designated variables is presented in Fig. 1. The sending end currents (i_A, i_B, i_C), receiving end currents (i_a, i_b, i_c), and receiving end voltages (v_a, v_b, v_c), are considered as the measurements in the state estimation (SE) problem, while the sending end voltages (v_A, v_B, v_C), and series branch currents (i_{dA}, i_{dB}, i_{dC}) are taken as the estimated variables in the SE problem. The selection of these variables as measurements and estimated variables is done on an arbitrary basis except the series branch currents (i_{dA}, i_{dB}, i_{dC}) which is due to their unavailability in the experimental setup. Any set of quantities could be chosen as measurements and estimated variables such that with a given selection of quantities, the state estimation remains an overdetermined problem. The series resistances of the three phases are represented as (R_A, R_B, R_C), inductances as (L_A, L_B, L_C), and capacitances as (C_A, C_B, C_C). (G_A, G_B, G_C) are not a part of the physical line model and are incorporated for the numerical stability of differential equations. When numerical integration is applied to differential equations, the incorporation of (G_A, G_B, G_C) helps in avoiding the expansion of round-off errors or fluctuations in the input data which might result in a considerable deviation of the final answer [18]. The dynamic modelling equations for phase A are presented as follows:

$$i_A + G_A v_a = i_{dA} + G_A v_A + C_A \frac{dv_A}{dt} \tag{1}$$

$$i_a - G_A v_a - C_A \frac{dv_a}{dt} = -i_{dA} - G_A v_A \tag{2}$$

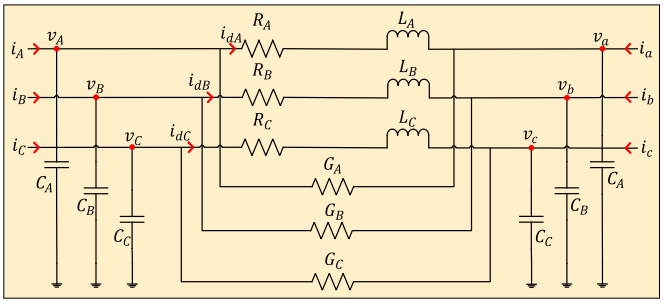

Fig. 1. Three-phase representation of a π-section of a transmission line.

$$v_a = v_A - R_A i_{dA} - L_A \frac{di_{dA}}{dt} \tag{3}$$

Along with phase B and C equations, (1)–(3) can be reformulated and can be expressed as follows:

$$R_1 z + R_2 \frac{dz}{dt} = S_1 x + S_2 \frac{dx}{dt} \tag{4}$$

where z is the measurement vector and x is the state vector, which can be expressed as:

$$z = \begin{bmatrix} i_A & i_B & i_C & i_a & i_b & i_c & v_a & v_b & v_c \end{bmatrix},$$
$$x = \begin{bmatrix} v_A & v_B & v_C & i_{dA} & i_{dB} & i_{dC} \end{bmatrix}$$

and R_1, R_2, S_1, and S_2, are the constant matrices formed with transmission line parameter values, which can be expressed as:

$$R_1 = \begin{bmatrix} 1&0&0&0&0&0&G_A&0&0 \\ 0&1&0&0&0&0&0&G_B&0 \\ 0&0&1&0&0&0&0&0&G_C \\ 0&0&0&1&0&0&-G_A&0&0 \\ 0&0&0&0&1&0&0&-G_B&0 \\ 0&0&0&0&0&1&0&0&-G_C \\ 0&0&0&0&0&0&1&0&0 \\ 0&0&0&0&0&0&0&1&0 \\ 0&0&0&0&0&0&0&0&1 \end{bmatrix}, R_2 = \begin{bmatrix} 0&0&0&0&0&0&0&0&0 \\ 0&0&0&0&0&0&0&0&0 \\ 0&0&0&0&0&0&0&0&0 \\ 0&0&0&0&0&0&-C_A&0&0 \\ 0&0&0&0&0&0&0&-C_B&0 \\ 0&0&0&0&0&0&0&0&-C_C \\ 0&0&0&0&0&0&0&0&0 \\ 0&0&0&0&0&0&0&0&0 \\ 0&0&0&0&0&0&0&0&0 \end{bmatrix}$$

$$S_1 = \begin{bmatrix} G_A&0&0&1&0&0 \\ 0&G_B&0&0&1&0 \\ 0&0&G_C&0&0&1 \\ -G_A&0&0&-1&0&0 \\ 0&-G_B&0&0&-1&0 \\ 0&0&-G_C&0&0&-1 \\ 1&0&0&-R_A&0&0 \\ 0&1&0&0&-R_B&0 \\ 0&0&1&0&0&-R_C \end{bmatrix}, S_2 = \begin{bmatrix} C_A&0&0&0&0&0 \\ 0&C_B&0&0&0&0 \\ 0&0&C_C&0&0&0 \\ 0&0&0&0&0&0 \\ 0&0&0&0&0&0 \\ 0&0&0&0&0&0 \\ 0&0&0&-L_A&0&0 \\ 0&0&0&0&-L_B&0 \\ 0&0&0&0&0&-L_C \end{bmatrix}$$

After obtaining (4) in the given form, QI method is applied to convert the differential equations into algebraic equations. QI method is applied over the two intervals $[t-k, t-k/2]$, and $[t-k, t]$, and the following equation is obtained:

$$H_1 \begin{bmatrix} z(t) \\ z\left(t-\frac{k}{2}\right) \end{bmatrix} = H_2 \begin{bmatrix} x(t) \\ x\left(t-\frac{k}{2}\right) \end{bmatrix} - H_3 [z(t-k)] - H_4 [x(t-k)] \tag{5}$$

where k is a one-time step of QI method, and matrices H_1, H_2, H_3, and H_4 are defined as follows.

$$H_1 = \begin{bmatrix} \frac{k}{6}R_1 + R_2 & \frac{2k}{3}R_1 \\ -\frac{k}{24}R_1 & \frac{k}{3}R_1 + R_2 \end{bmatrix}, H_2 = \begin{bmatrix} \frac{k}{6}S_1 + S_2 & \frac{2k}{3}S_1 \\ -\frac{k}{24}S_1 & \frac{k}{3}S_1 + S_2 \end{bmatrix}$$
$$H_3 = \begin{bmatrix} \frac{k}{6}R_1 - R_2 \\ \frac{5k}{24}R_1 - R_2 \end{bmatrix}, H_4 = \begin{bmatrix} -\frac{k}{6}S_1 + S_2 \\ -\frac{5k}{24}S_1 + S_2 \end{bmatrix}$$

The detailed derivation and explanation of the QI method are presented in [18], AQCF model in [19], and transmission line dynamic modelling along with the derivation of matrices H_1, H_2, H_3, and H_4 are presented in [20].

The restructuring of (5) in the standard form of the SE equation, gives the following:

$$\begin{bmatrix} z(t) \\ z\left(t-\frac{k}{2}\right) \end{bmatrix} = H \begin{bmatrix} x(t) \\ x\left(t-\frac{k}{2}\right) \end{bmatrix} + C \tag{6}$$

where $H = H_1^{-1} H_2$, $C = -C_1 [z(t-k)] - C_2 [x(t-k)]$, $C_1 = H_1^{-1} H_3$, $C_2 = H_1^{-1} H_4$.

2.2.2. State estimation

The linear version of the weighted least square (WLS) algorithm is used for solving the state estimation problem and can be stated as:

$$z = Hx + \eta \tag{7}$$

where z represents the measurement vector consisting of sampled values of voltages and currents, H represents the Jacobian matrix, x represents the state vector and η represents the measurement error vector.

2.2.3. Chi-square test

For the quantification of the confidence level, the Chi-square test is used which requires the degree of freedom and state estimation objective function as inputs. The following steps are involved:

- Calculation of state estimation objective function which is defined as

$$J = (z - H\hat{x})^T W^{-1} (z - H\hat{x}) = \eta^T W^{-1} \eta \tag{8}$$

  where, $\hat{x}$ is the WLS estimate, W^{-1} is the diagonal weight matrix and defined as

$$diag\left(\sigma_1^2, \sigma_2^2, \sigma_3^2, \ldots, \sigma_m^2\right)$$

  and σ_i represents the standard deviation of each measurement i. The standard maximum measurement uncertainties associated with the voltage and current (PMU) measurements considered in this work are presented in Table 1 [21,22].
- The confidence level is quantified based on state estimation objective function J and degree of freedom (d) which is defined as $d = m - n$, where m is the number of measurements and n is the number of state variables. Thereafter, the Chi-square distribution table is checked for quantification of the confidence level.

Table 1
Standard maximum measurement uncertainties associated with different types of PMU measurements.

Measurement type	Voltage	Current
Maximum uncertainty	0.02%	0.03%

2.2.4. Confidence level

The evaluation of confidence level (h) in transmission line health is done based on the goodness of fit between the transmission line dynamic model and measurements obtained from the Chi-square test, as below:

$$h = 1 - p_{[\chi^2 \leq J]} \tag{9}$$

where, $p_{[\chi^2 \leq J]}$ is the probability of the χ^2 distribution for $\chi^2 \leq J$.

2.2.5. Threshold value and low pass filter

A threshold value is required to be selected to bring the state estimation objective function values to zero so that the confidence level remains high during normal operating conditions. The main reason behind the threshold value is the mismatch that occurs between the measurements and their estimated values, and it leads to non-zero finite values of the state estimation objective function. The basis for the selection of the threshold value is the range of the objective function values obtained during normal operating conditions with due consideration of the measurement uncertainties and any changes in network configuration. The credible way of obtaining a threshold value that works in most cases is simulating a case with maximum fault current and then validating whether it works in other cases such as external

faults, and minimum fault current with the highest fault impedance and weakest source. Further, it should be verified that the tripping is not initiated during high load conditions, instrumentation errors, and current transformer saturation. From the experience of validations with various types of faults carried out in this paper using the scaled-down model of a 150-km 400 kV (L-L) transmission line under the given load conditions, the threshold value ranges between 30e3 to 40e3, while the maximum measurement uncertainties were in the range of 0.02% and 0.03%. In addition to the threshold value, a low pass filter is also used for smoothing and avoiding any unreasonable spike in the objective function curve. The following low pass filter is employed:

$$J^{f}_{new} = (\alpha \times J) + \left[(1-\alpha) \times J^{f}_{previous}\right] \tag{10}$$

where α is the smoothing factor which varies between 0 and 1, J and J^{f} are the original and new objective functions, respectively. This work considers the value of α as 0.09 which is based on the experience from the different case studies carried out in this work. All the following objective function plots presented in the paper involve the application of a low pass filter.

3. Description of Experimental Setup and Implementation of DSEBPS

This section presents a detailed explanation of the case study used in the experimental validation of DSEBPS. The subsections present the details of advanced sensors and their usage, the laboratory and experimental setup details, the implementation of the scheme, and the trip signal logic.

3.1. Advanced sensors usage

Advanced sensors have been continuously developed by Smart State Technology [23]. They provide real-time global positioning system (GPS) synchronized sampled measurements which are required as inputs to DSE. The quality (i.e., accuracy, time synchronization, and sampling frequency) of the sampled measurements is the backbone of DSEBPS and thus it is an important requirement for the accurate and timely detection of the fault. Advanced sensors provided sampled measurements at the frequency of 4 kHz i.e., one sample in 250 μs. The high sampling frequency of GPS-synchronized measurements ensures the proper capturing of any dynamical change in the network. This work employs three advanced sensors, out of which two are current sensors and one is a voltage sensor. They provide voltage and current measurements that constitute the measurement vector which is represented as z in (7).

3.2. Laboratory and experimental setup description

A physical setup available at the Chalmers power system laboratory consisting of six π-sections of transmission line, transformers, synchronous generator, and loads, is considered in this work. The setup is an accurate scaled-down model of a power system where each π-section represents 150 km of a 400 kV transmission line. The per-phase parameters for each π-section are as follows: resistance 0.052 Ω, inductance 3.033 mH, and capacitance 46 μF. The synchronous generator has a rated three-phase voltage of 400 V and is driven by an 85 kW DC motor (which functions as a prime mover). The setup is connected to a three-phase 400 V (L-L), 50 Hz distribution grid on the grid end. The setup also contains two three-phase transformers, one on the generator end which has a YD11 connection with Y-connection on the transmission line side and D-connection on the generator side. The other transformer is on the grid end which has a DYn11 connection with D-connection on the grid side and Yn-connection on the transmission line side. The entire setup is solidly grounded through a copper strip for safety purposes. Various types of loads could be connected with the setup at different locations. The laboratory has a provision to create temporary (self-clearing) faults using a timer and push button. Advanced sensors used in the experimental setup measure sending end currents (i_A, i_B, i_C), receiving end currents (i_a, i_b, i_c), and receiving end voltages (v_a, v_b, v_c). The current sensors employ split-core current transformers (CTs) of the measurement class with a current range from normal operating current to maximum fault current. The voltage sensors directly measure the voltage without employing the voltage transformers.

3.3. Implementation

The implementation diagram of DSEBPS with the experimental setup is shown in Fig. 2. The real-time sampled measurements are received by the smart node (a laptop in this setup) by installing advanced sensors at the transmission line. The configuration details of the laptop used in the setup are presented in [17]. The measurements are processed along with the transmission line dynamic model to perform DSE. The state estimates are obtained using DSE after which the Chi-square test is performed to obtain the goodness of fit between the transmission line dynamic model and measurements. The results obtained for the goodness of fit are used to derive the health condition of the transmission line and subsequently the confidence level. Finally, the confidence level helps in designing the protection logic and issuing a trip signal.

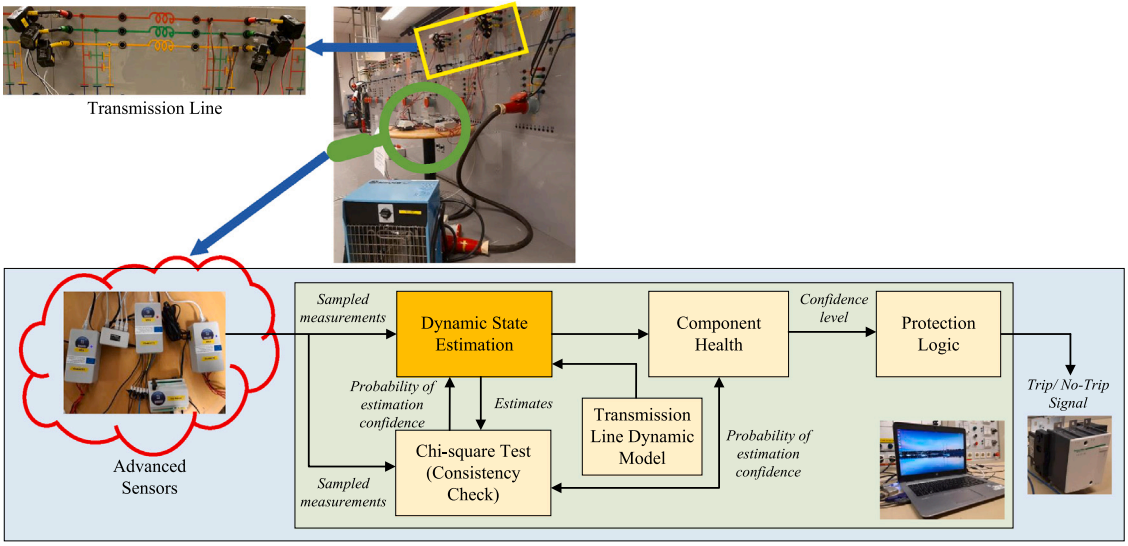

Fig. 2. Implementation figure of DSEBPS with the experimental setup.

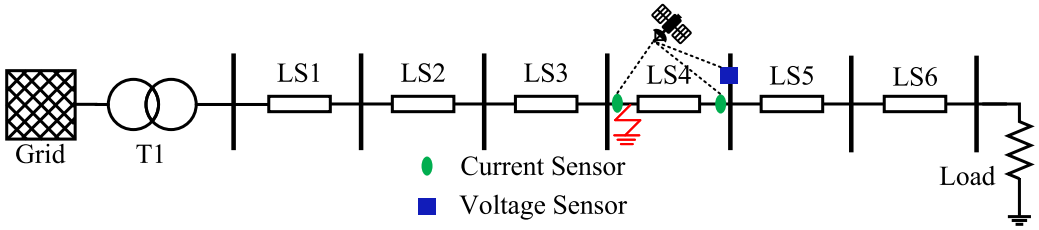

Fig. 3. Schematic of the experimental setup for an unbalanced fault.

3.4. Trip signal logic

The consistency of the objective function is used to obtain the confidence level which in turn is used to generate the trip signal. In order to generate the trip signal, the confidence level signal should be low. The objective function is observed for forty consecutive samples (or any desired number of samples by the user) to be above a threshold value and then the confidence level signal goes low. The motivation to observe the objective function for forty consecutive samples is to obtain enhanced reliability of the protection decision. Once the trip signal is generated, it is sent to the circuit breakers which isolate the transmission line from the rest of the network.

4. Performed test cases: Results and discussion

4.1. Unbalanced faults

This subsection presents the results of the unbalanced faults using the experimental setup which is explained in Section 3. The schematic of the experimental setup in case of an unbalanced fault is presented in Fig. 3. In this section, the results for two unbalanced faults i.e., single-line-to-ground and double-line-to-ground faults, are presented.

4.1.1. Single-line-to-ground fault

A single-line-to-ground fault is the most common and frequently occurring fault type in transmission systems. The sampled measurements are received at a sampling frequency of 4 kHz, or each sampled measurement is received in 250 μs. The validation results in terms of measured and estimated values of sending end currents (i_A, i_B, i_C), receiving end currents (i_a, i_b, i_c), and receiving end voltages (v_a, v_b, v_c) are presented in Fig. 4. The objective function and confidence level results are presented in Fig. 5. The measurements, estimated values, objective function, and confidence level are obtained continuously and plotted in Fig. 4 and Fig. 5. As can be seen from Fig. 4, during the normal operating conditions (until 4.95 s) the measured and estimated values are in concurrence with each other. The concurrency between the measured and their estimated values signify the correct modelling of the transmission line. Consequently, the objective function has lower values, and the confidence level remains high.

Thereafter, a single-line-to-ground fault is created in phase A (at sending end of the fourth π-section) for 40 ms at around 4.95 s. It can be seen from Fig. 4 that during the fault the sending end current in phase A (i_A) increases significantly and reaches a peak value up to 130 Amperes (as it is the faulted phase), while the sending end currents in other phases (i_B and i_C) see some distortions during the fault as they are healthy phases. The receiving end current in phase A (i_a) reduces during the fault as the short circuit fault occurs before the receiving end and part of the current is fed to the fault, while the receiving end currents in other phases (i_b and i_c) see a very small dip in currents as they are healthy phases. Conversely, the receiving end voltage in phase A (v_a) reduces to zero during the fault because the fault occurs with a zero impedance path, and hence the voltage becomes close to zero at the fault point, while the receiving end voltages in healthy phases (v_b and v_c) see an increase because the grid-end transformer in the lab setup has DYn11 winding connection with the neutral of the secondary side solidly grounded which gives a ground path to the zero-sequence

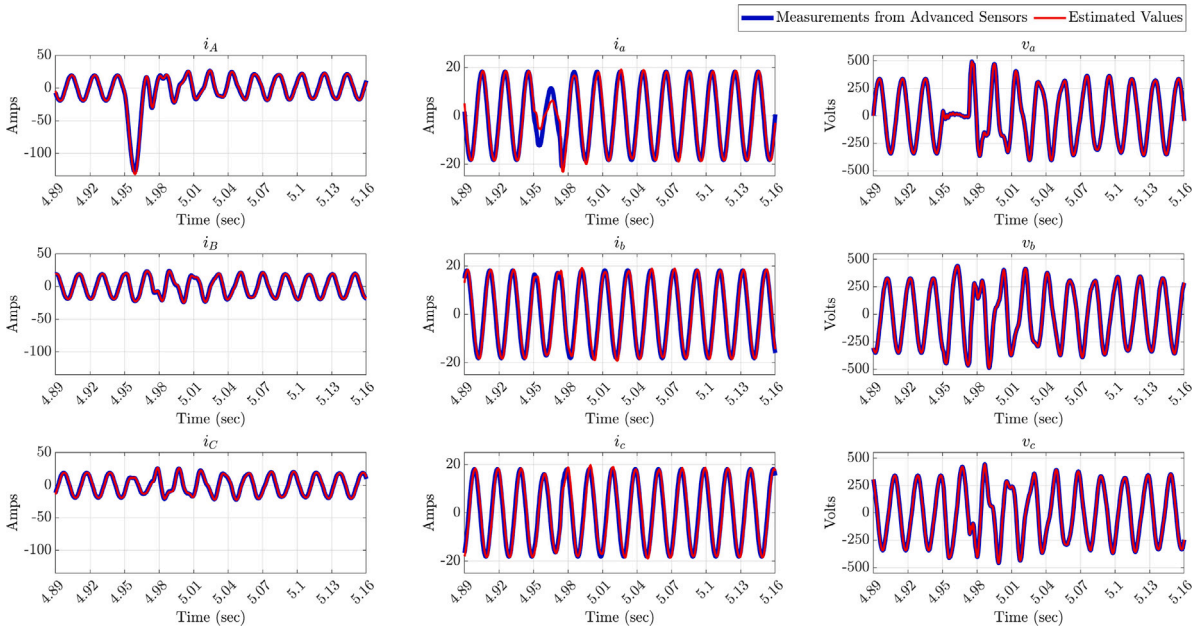

Fig. 4. Validation results for a single line-to-ground fault in terms of measured and estimated values of the sending end currents (i_A, i_B, i_C), receiving end currents (i_a, i_b, i_c), and receiving end voltages (v_a, v_b, v_c).

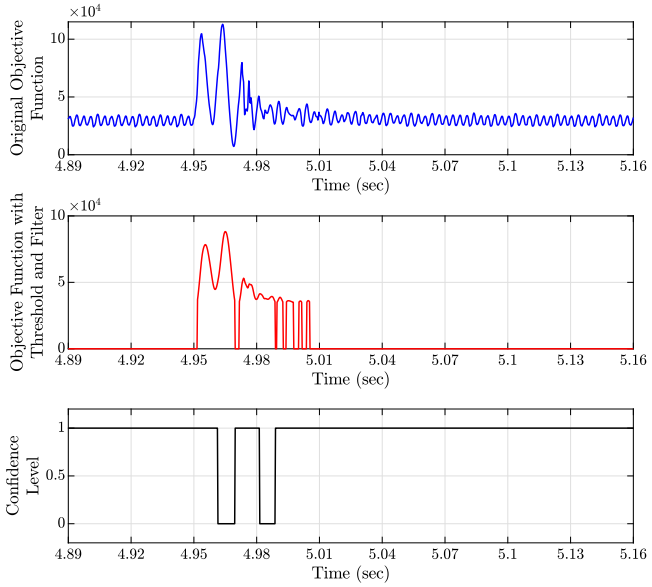

Fig. 5. Validation results for a single line-to-ground fault in terms of objective function and confidence level.

current to flow and hence the voltages in healthy phases are affected. Further, it can be seen from Fig. 5 that as soon as the single-line-to-ground fault occurs at around 4.95 s the objective function goes higher than the threshold value of 35e3, and subsequently, the confidence level goes low (i.e., 0) after 40 samples (10 ms) at around 4.96 s. The low confidence level generates a trip signal to isolate the fault. The results obtained from the case study suggest that DSEBPS works as intended during a single-line-to-ground fault.

4.1.2. Double-line-to-ground fault

A double-line-to-ground fault involves any of the two phases and ground during the fault conditions. The validation results in terms of measured and estimated values of sending end currents (i_A, i_B, i_C), receiving end currents (i_a, i_b, i_c), and receiving end voltages (v_a, v_b, v_c) are presented in Fig. 6. The objective function and confidence level results are presented in Fig. 7. The measurements, estimated values, objective function, and confidence level are obtained continuously and plotted in Fig. 6 and Fig. 7. As can be seen from Fig. 6, during the normal operating conditions (until 2.76 s) the measured and estimated values are in concurrence with each other. The concurrency between the measured and their estimated values proves the correct modelling of the transmission line. Consequently, the objective function has lower values and the confidence level is high until 2.76 s.

Thereafter, a double-line-to-ground fault is created in phases A and B (at sending end of the fourth π-section) for 40 ms at around 2.76 s. It can be seen from Fig. 6 that during the fault the sending end currents in phases A and B (i_A and i_B) increase significantly and reaches a peak value up to 130 Amperes (as they are the faulted phases), while the sending end current in phase C (i_C) see some distortions during the fault as it is the healthy phase. The receiving end currents in phases A and B (i_a and i_b) reduce during the fault as the short circuit fault occurs before the receiving end and part of the current is fed to the fault, while the receiving end current in phase C (i_c) see a very small reduction in current as it is the healthy phase. Conversely, the receiving end voltages in phases A and B (v_a and v_b) reduce to zero during the fault because the fault occurs with a zero impedance path, and hence the voltage reaches close to zero at the fault point, while the receiving end voltage in the healthy phase (v_c) see an increase because the grid-end transformer in the lab setup has DYn11 winding connection with the neutral of the secondary side solidly grounded which gives a ground path to the zero-sequence current to flow and hence the voltage in healthy phase is affected. Further, it can be seen from Fig. 7 that as soon as the double-line-to-ground fault occurs at around 2.76 s the objective function goes higher than the threshold value of 35e3, and subsequently, the confidence level goes low after 40 samples at around 2.77 s. The low confidence level generates a trip signal to clear the fault. The results suggest that DSEBPS successfully detects the double-line-to-ground fault.

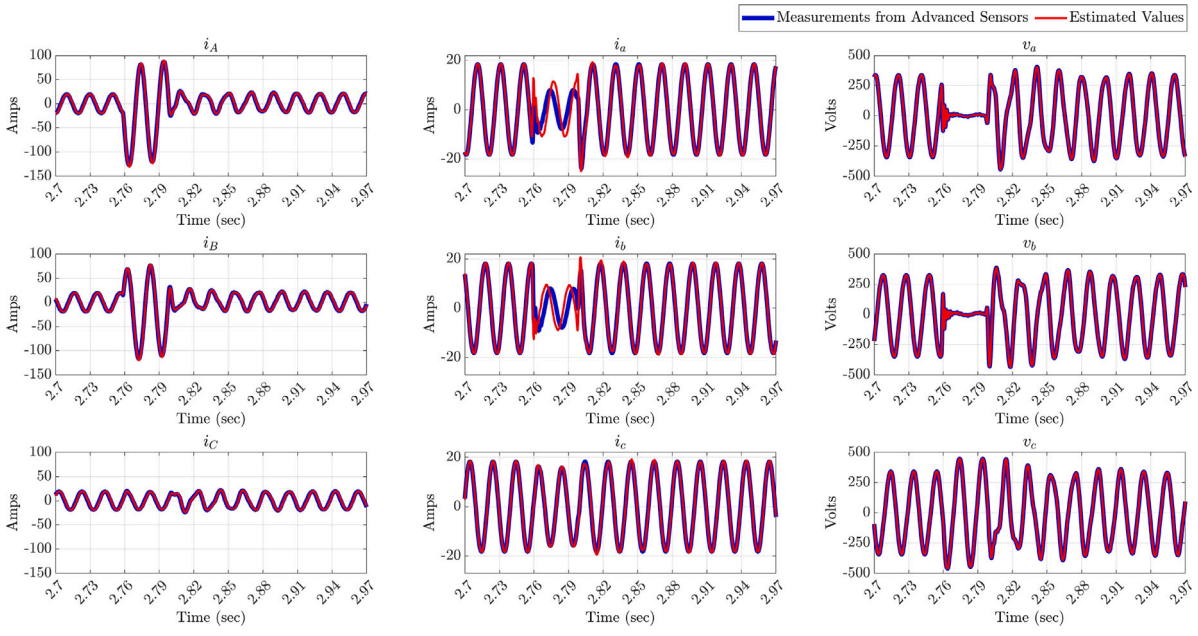

Fig. 6. Validation results for a double line-to-ground fault in terms of measured and estimated values of the sending end currents (i_A, i_B, i_C), receiving end currents (i_a, i_b, i_c), and receiving end voltages (v_a, v_b, v_c).

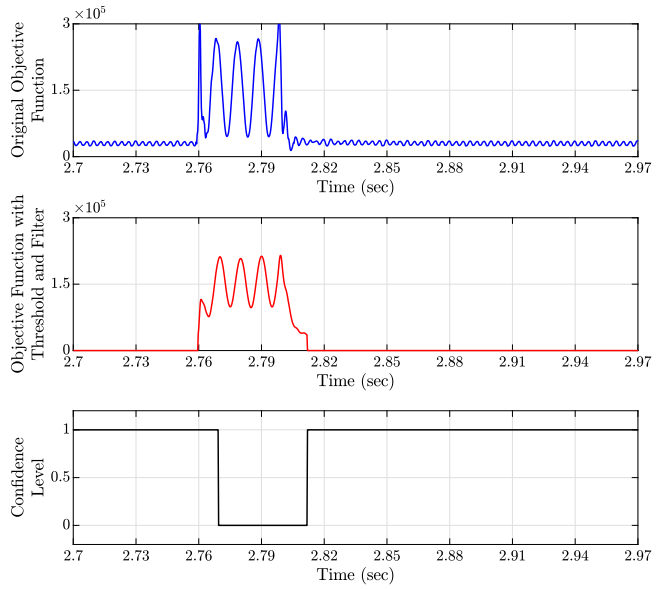

Fig. 7. Validation results for a double line-to-ground fault in terms of objective function and confidence level.

4.2. Unbalanced fault with different load conditions

Power systems mostly operate with inductive power factor load conditions. The inductive load conditions not just make the system response to disturbances more sluggish due to increased time constant but also increases the phase difference between the voltage and current (compared to resistive load). Due to this different protection settings are required in some phasor-based protection methods such as distance and directional overcurrent, as the decision is based on both the magnitude and angle of the phasor. In this regard, this case study is performed to validate the performance of DSEBPS under inductive load conditions. The picture showing the experimental setup for the inductive load conditions is presented in Fig. 9(a). DSEBPS is validated with an inductive load of 0.78 power factor (2.2 kW and 1.7 kVAr) using the same experimental setup. The validation results in terms of measured and estimated values of sending end current (i_A), receiving end current (i_a), and receiving end voltage (v_a) for phase A, are presented in Fig. 8. The objective function and confidence level results are presented in Fig. 9(b). The measurements, estimated values, objective function, and confidence level are obtained continuously and plotted in Fig. 8 and Fig. 9(b). As can be seen from Fig. 8, during the normal operating conditions (until 2.47 s) the measured and estimated values are in concurrence with each other. The concurrency between the measured and their estimated values signify the correct modelling of the transmission line. Consequently, the objective function has lower values, and the confidence level is high until 2.47 s.

Thereafter, a single-line-to-ground fault is created in phase A (at sending end of the fourth π-section) for 40 ms at around 2.47 s. It can be seen from Fig. 8 that during the fault the sending end current in phase A (i_A) increases significantly and reaches a peak value of 130 Amperes (as it is the faulted phase), while the sending end currents in other phases (i_B and i_C) see some distortions during the fault as they are healthy phases. The receiving end current in phase A (i_a) reduces during the fault as the short circuit fault occurs before the receiving end and part of the current is fed to the fault, while the receiving end currents in other phases (i_b and i_c) see a very small dip in currents as they are healthy phases. Conversely, the receiving end voltage in phase A (v_a) reduces to zero during the fault because the fault occurs with a zero impedance path and hence the voltage becomes close to zero at the fault point, while the receiving end voltages in healthy phases (v_b and v_c) see an increase because the grid-end transformer in the lab setup has DYn11 winding connection with the neutral of the secondary side solidly grounded which gives a ground path to the zero-sequence current to flow and hence the voltages in healthy phases are affected. Further, it can be seen from Fig. 9(b) that immediately after the occurrence of a single-line-to-ground fault at around 2.47 s, the objective function goes higher than the threshold value of 35e3, and subsequently, the confidence level goes low (i.e., 0) after 40 samples at around 2.48 s. The low confidence level leads to the generation of a trip signal and hence the fault is successfully detected. It is important to highlight here that the transient response of the system to the fault with inductive load is a little sluggish when compared to the system with purely resistive load. However, the results affirmed that the difference

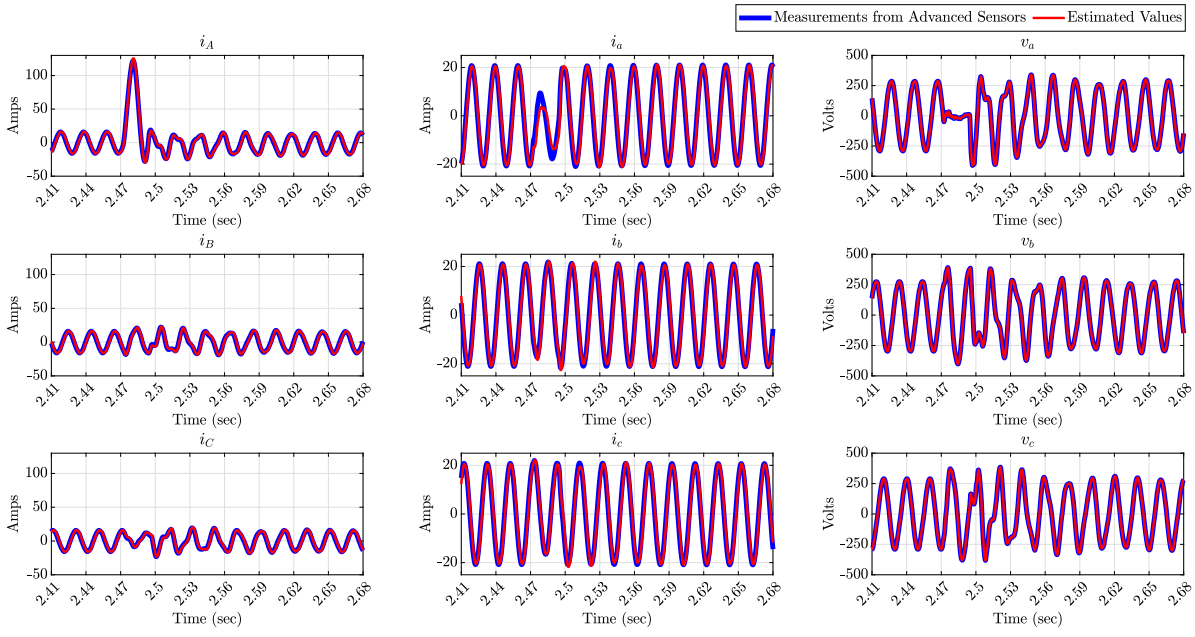

Fig. 8. Validation results for a single line-to-ground fault with R-L load in terms of measured and estimated values of the sending end currents (i_A, i_B, i_C), receiving end currents (i_a, i_b, i_c), and receiving end voltages (v_a, v_b, v_c).

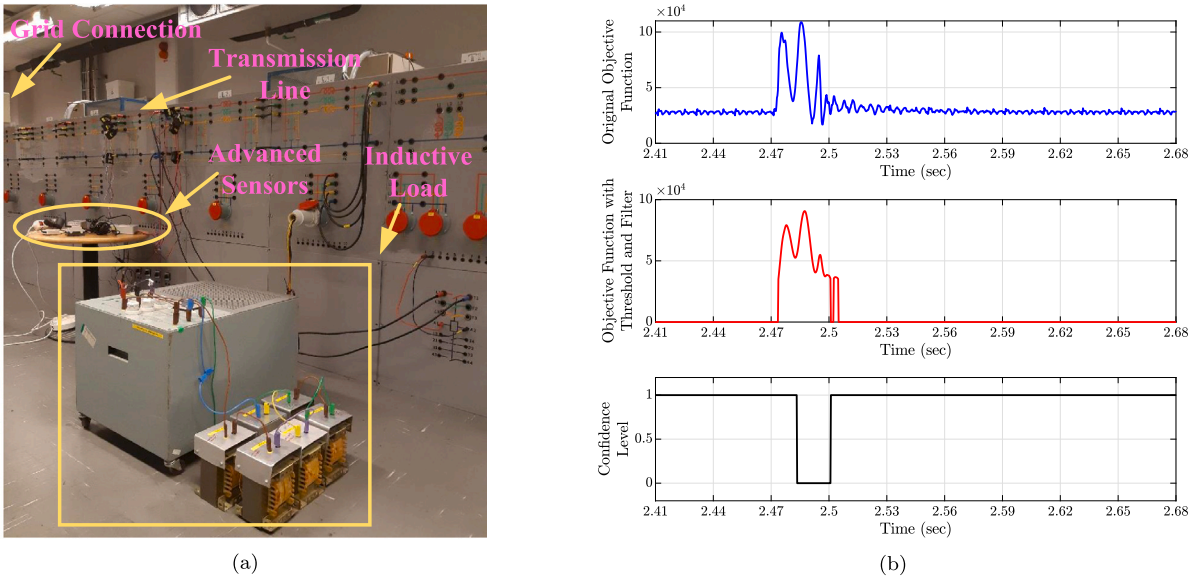

Fig. 9. Inductive Load - (a) Picture showing the experimental setup of DSEBPS and (b) Objective function and confidence level results in case of a single line-to-ground fault.

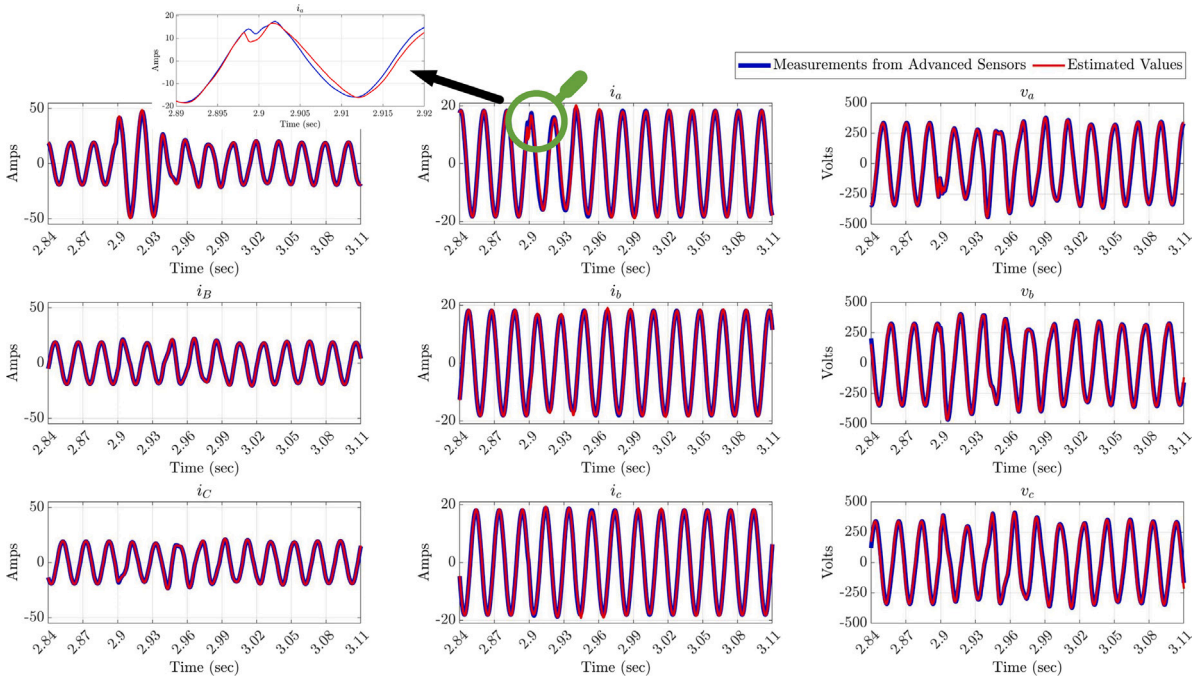

Fig. 10. Validation results for a single line-to-ground fault with high impedance in terms of measured and estimated values of the sending end currents (i_A, i_B, i_C), receiving end currents (i_a, i_b, i_c), and receiving end voltages (v_a, v_b, v_c).

in system response does not have any impact on the performance of DSEBPS. The fault is detected and cleared well within the standard fault-clearing time and does not require any changes in this case. The results from the case study confirm the intended performance of DSEBPS with the inductive load as well.

4.3. High impedance fault

A high impedance fault can be classified as a fault that includes high impedance in the fault path. The high impedance fault path distinguishes it from the low impedance fault path as the fault current is reduced significantly, sometimes close to or less than the normal operating conditions. The reduced fault current makes it difficult to detect and clear the fault. The picture showing the experimental setup for a high impedance fault is presented in Fig. 11(a). DSEBPS is validated for a high impedance (single-line-to-ground) fault using the same experimental setup. The validation results in terms of measured and estimated values of sending end currents (i_A, i_B, i_C), receiving end currents (i_a, i_b, i_c), and receiving end voltages (v_a, v_b, v_c) are presented in Fig. 10. The objective function and confidence level results are presented in Fig. 11(b). The measurements, estimated values, objective function, and confidence level are obtained continuously and plotted in Fig. 10 and Fig. 11(b). As can be seen from Fig. 10, during the normal operating conditions (until 2.90 s) the measured and estimated values are in concurrence with each other. The concurrency between the measured and their estimated values indicates the correct modelling of the transmission line. Consequently, the objective function has lower values and the confidence level is high.

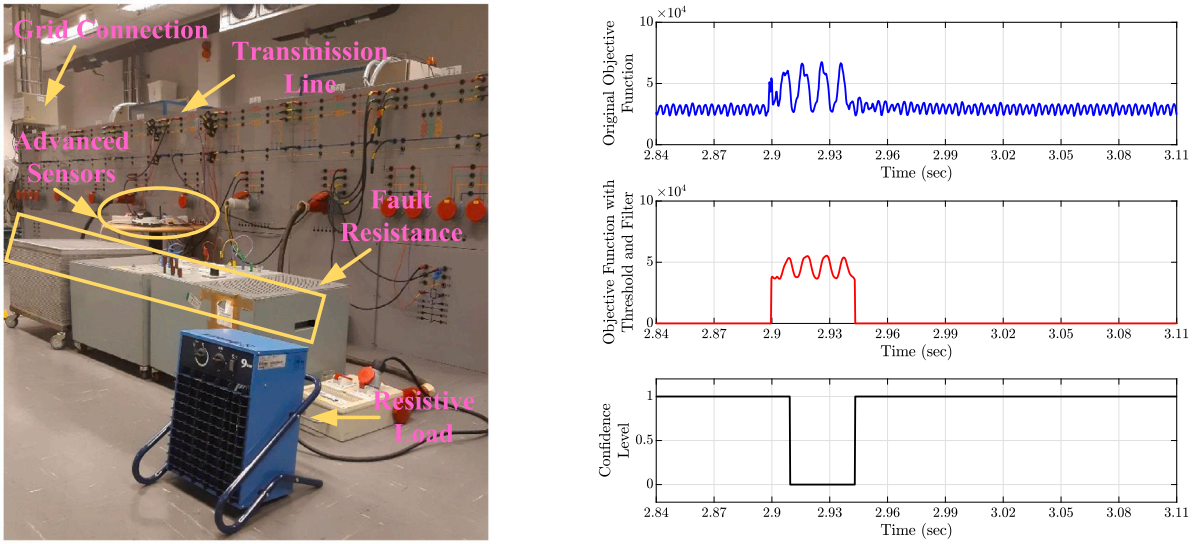

Fig. 11. High Impedance Fault - (a) Picture showing the experimental setup of DSEBPS and (b) Objective function and confidence level results in case of a single line-to-ground fault.

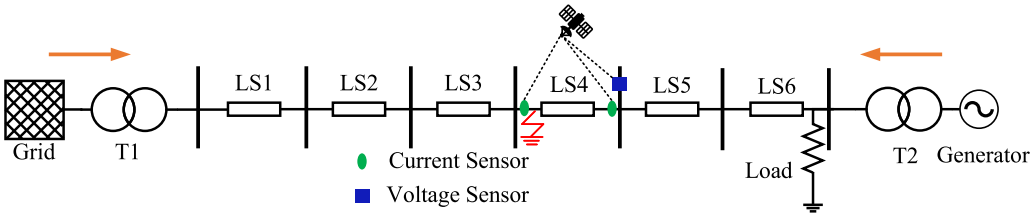

Fig. 12. Schematic of the experimental setup for a fault current fed from both ends.

Thereafter, a single-line-to-ground fault with a fault impedance of 9 Ω is created in phase A (at sending end of the fourth π-section) for 40 ms at around 2.90 s. It can be seen from Fig. 10 that during the fault the sending end current in phase A (i_A) does not increase significantly (compared to a single-phase-to-ground fault with a low impedance fault path) as the fault path has increased impedance and reduced current is fed to the fault and reaches a peak value of 50 Amperes (compared to 130 Amperes in a single-phase-to-ground fault with zero fault impedance), while the sending end currents in other phases (i_B and i_C) see some distortions during the fault as they are healthy phases. The receiving end current in phase A (i_a) sees a slight reduction during the fault as the fault current has reduced compared to a case with zero impedance fault, while the receiving end currents in other phases (i_b and i_c) remain close to normal operating value due to lesser fault effects on the faulted phase. Conversely, the receiving end voltage in phase A (v_a) does not reduce to zero during the fault (compared to a single-phase-to-ground fault with zero fault impedance), while the receiving end voltages in other phases (v_b and v_c) see a slight spike. Further, it can be seen from Fig. 11(b) that as soon as the single-line-to-ground fault occurs at around 2.90 s the objective function goes higher than the threshold value of 35e3, and subsequently, the confidence level goes low (i.e., 0) after 40 samples at around 2.91 s. However, it can be observed that the spike in the objective function is lower than the objective function obtained with a single-line-to-ground fault with zero fault impedance. But since the confidence level signal is based on the consistency of the objective function, thus when the objective function remains above (crosses) the threshold value for 40 samples, the confidence level goes low (i.e., 0). The low confidence level generates a trip signal and hence the fault is successfully detected. It is important to highlight here that DSEBPS performs as intended during a high impedance fault and hence affirms it is one of the significant features.

4.4. Fault current fed from both ends

Transmission systems are generally connected as meshed networks where the fault is fed from both ends of the transmission line. The schematic of the system with a fault current fed from both ends is presented in Fig. 12, while the corresponding experimental setup is presented in Fig. 14(a).

The validation results in terms of measured and estimated values of sending end currents (i_A, i_B, i_C), receiving end currents (i_a, i_b, i_c), and receiving end voltages (v_a, v_b, v_c) are presented in Fig. 13. The objective function and confidence level results are presented in Fig. 14(b). The measurements, estimated values, objective function, and confidence level are obtained continuously and plotted in Fig. 13 and Fig. 14(b). All the plots in Fig. 13 show that during the normal operating conditions (until 1.03 s) the measured and estimated values are in concurrence with each other signifies the correct modelling of the transmission line. Consequently, the objective function has lower values, and the confidence level is high until 1.03 s in Fig. 14(b).

Thereafter, a three-phase fault is created (at sending end of the fourth π-section) for 40 ms at around 1.03 s. It can be seen from Fig. 13 that during the fault the sending end currents (i_A, i_B, i_C) increase significantly and reach a peak value up to 180 Amperes as the fault path has zero impedance which leads to high fault current. The receiving end currents (i_a, i_b, i_c) also increase during the fault (unlike the fault current fed from one end) as the fault current is fed from both ends

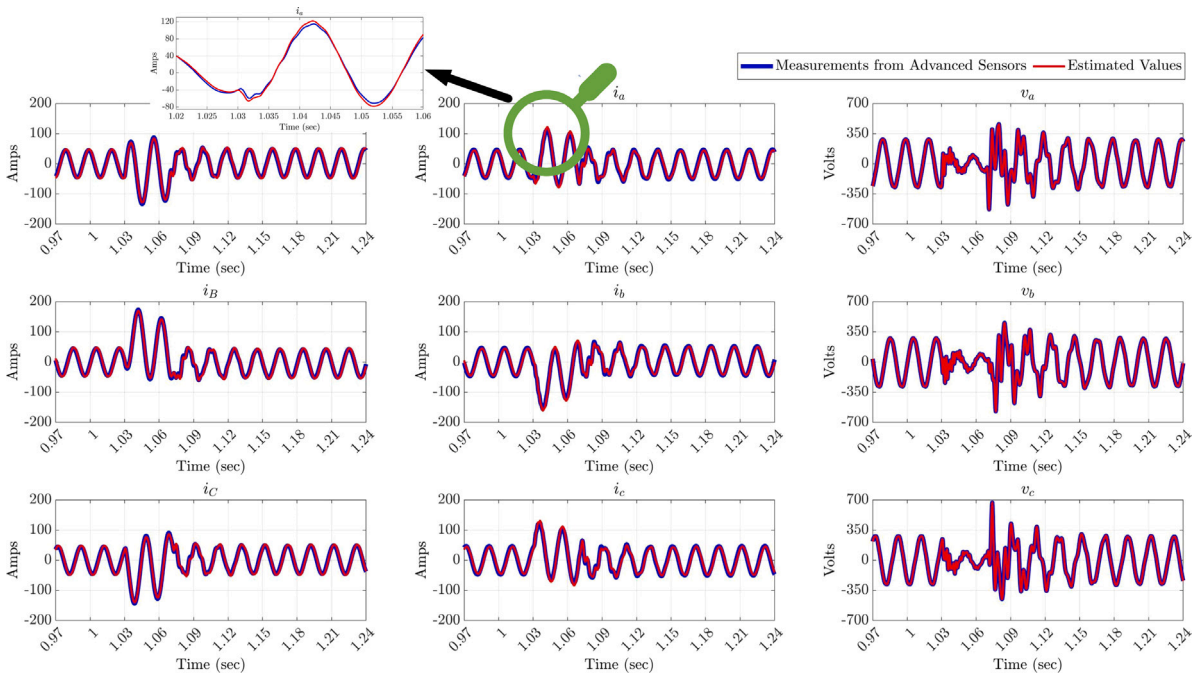

Fig. 13. Validation results for a three-phase fault current fed from both ends in terms of measured and estimated values of the sending end currents (i_A, i_B, i_C), receiving end currents (i_a, i_b, i_c), and receiving end voltages (v_a, v_b, v_c).

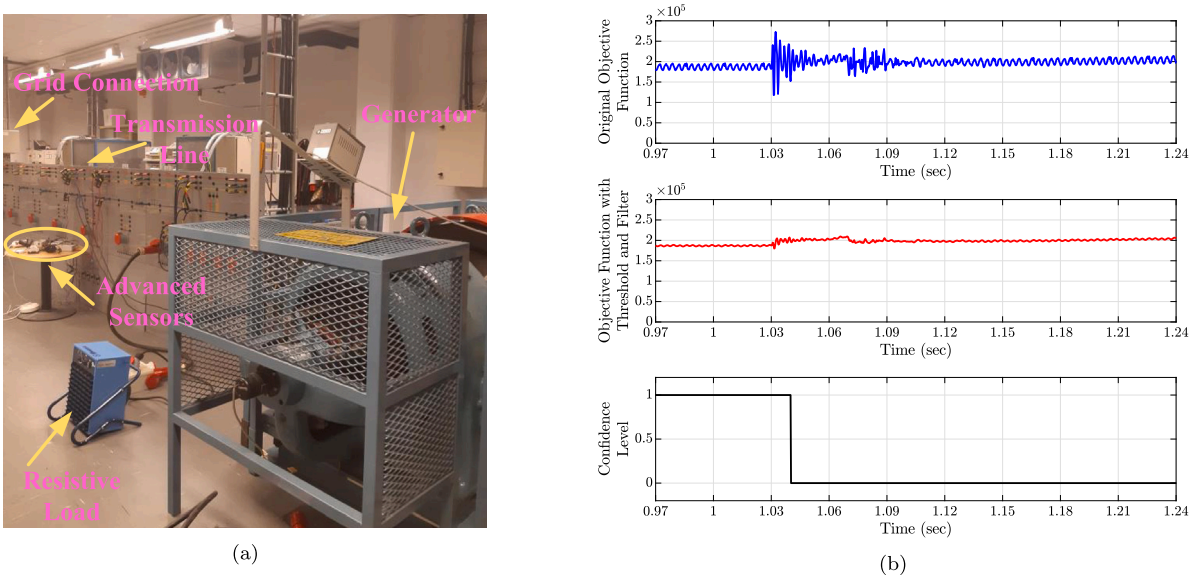

Fig. 14. Fault Fed from Both Ends - (a) Picture showing the experimental setup of DSEBPS and (b) Objective function and confidence level results in case of a three-phase fault.

and thus generator also contributes to the fault current leading to the high current on the receiving end. In the case of the receiving end voltages (v_a, v_b, v_c) a reduction can be seen during the fault but they are not reduced to zero unlike the fault current fed from one end as the corresponding receiving end current is not zero as fault current is fed from both ends. Further, it can be seen from Fig. 14(b) that as soon as the three-phase fault occurs at around 1.03 s, the objective function goes higher than the threshold value, and subsequently, the confidence level goes low (i.e., 0) after 40 samples at around 1.04 s. The low confidence level generates a trip signal and hence the fault is successfully detected. However, a different value of the threshold value i.e., 189e3 is used in this case study as the network configuration is changed due to the addition of a generator. This case study demonstrated the expected performance of DSEBPS during the condition where the fault current is fed from both ends.

4.5. Hidden failure

Hidden failure can be described as one which could be caused due to failure of instrument transformers, or human errors such as wrong connections, incorrect settings, etc. In this case study, DSEBPS is validated with the same experimental setup for a case of a hidden failure where a CT connected to sending end side of phase B is considered as failed. The validation results in terms of measured and estimated values of sending end currents (i_A, i_B, i_C), receiving end currents (i_a, i_b, i_c), and receiving end voltages (v_a, v_b, v_c) are presented in Fig. 15. The objective function and confidence level results are presented in Fig. 16. The

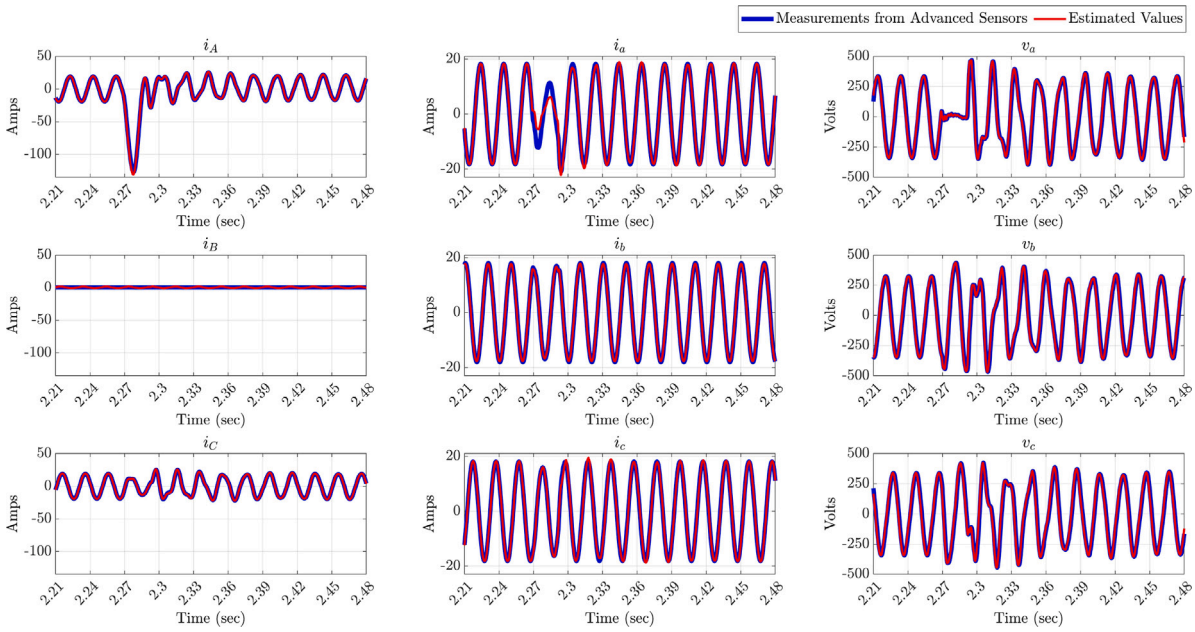

Fig. 15. Validation results for a hidden failure in terms of measured and estimated values of the sending end currents (i_A, i_B, i_C), receiving end currents (i_a, i_b, i_c), and receiving end voltages (v_a, v_b, v_c).

measurements, estimated values, objective function, and confidence level are obtained continuously and plotted in Fig. 15 and Fig. 16. As can be seen from Fig. 15, due to consideration of CT failure connected to sending end of phase B, the measurements are not received, and consequently, the estimated values are also not obtained. However, the corresponding plot shows the noise values associated with that measurement. The other plots in Fig. 15 show that during the normal operating conditions (until 2.27 s) the measured and estimated values are in concurrence with each other. The concurrency between the other measurements and their estimated values indicates the correct modelling of the transmission line. Consequently, the objective function has lower values, and the confidence level is high until 2.27 s.

Thereafter, a single-phase-to-ground fault is created (at sending end of the fourth π-section) for 40 ms at around 2.27 s. It can be seen from Fig. 16 that during the fault the sending end current in phase A (i_A) reaches a peak value of 130 Amperes (as it is the faulted phase), sending end current in phase C (i_C) slightly decreases while sending end current in phase B (i_B) does not change. The receiving end currents in all the phases (i_a, i_b, i_c) see a slight reduction during the fault as the short circuit fault occurs before the receiving end and part of the current is fed to the fault. Also, the receiving end voltage in phase A (v_a) reduces to zero during the fault because the fault occurs with a zero impedance path, and hence the voltage becomes close to zero at the fault point, while the receiving end voltages in healthy phases (v_b and v_c) see an increase because the grid-end transformer in the lab setup has DYn11 winding connection with the neutral of the secondary side solidly grounded which gives a ground path to the zero-sequence current to flow and hence the voltages in healthy phases are affected. Further, it can be seen from Fig. 16 that as soon as the single-phase-to-ground fault occurs at around 2.27 s, the objective function goes higher than the threshold value of 35e3, and subsequently, the confidence level goes low (i.e., 0) after 40 samples at around 2.28 s. The low confidence level generates a trip signal and hence the fault is successfully detected and cleared. It is important to highlight here that despite the hidden failure (in CT of sending end side of phase B), the fault is detected and cleared within the standard fault clearing time. The results from the case study suggest that DSEBPS performed as expected in case of a hidden failure and thereby confirming its robustness.

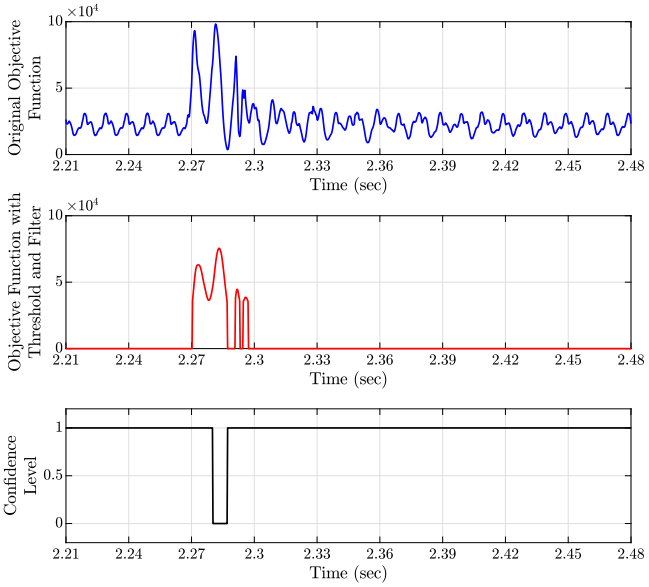

Fig. 16. Validation results for a hidden failure in terms of objective function and confidence level.

4.6. External fault

An external fault is one that does not occur inside the designated protection zone implying that it should not be detected as an internal fault and hence a trip signal should not be generated. In this case study, DSEBPS is validated for a case of an external fault (at receiving end of the third π-section). The validation results in terms of measured and estimated values of sending end currents (i_A, i_B, i_C), receiving end currents (i_a, i_b, i_c), and receiving end voltages (v_a, v_b, v_c) are presented in Fig. 17. The objective function and confidence level results are presented in Fig. 18. The measurements, estimated values, objective function, and confidence level are obtained continuously and plotted in Fig. 17 and Fig. 18. As the external fault occurs at approximately 1.56 s, the transients in the currents and voltages can be seen in Fig. 17.

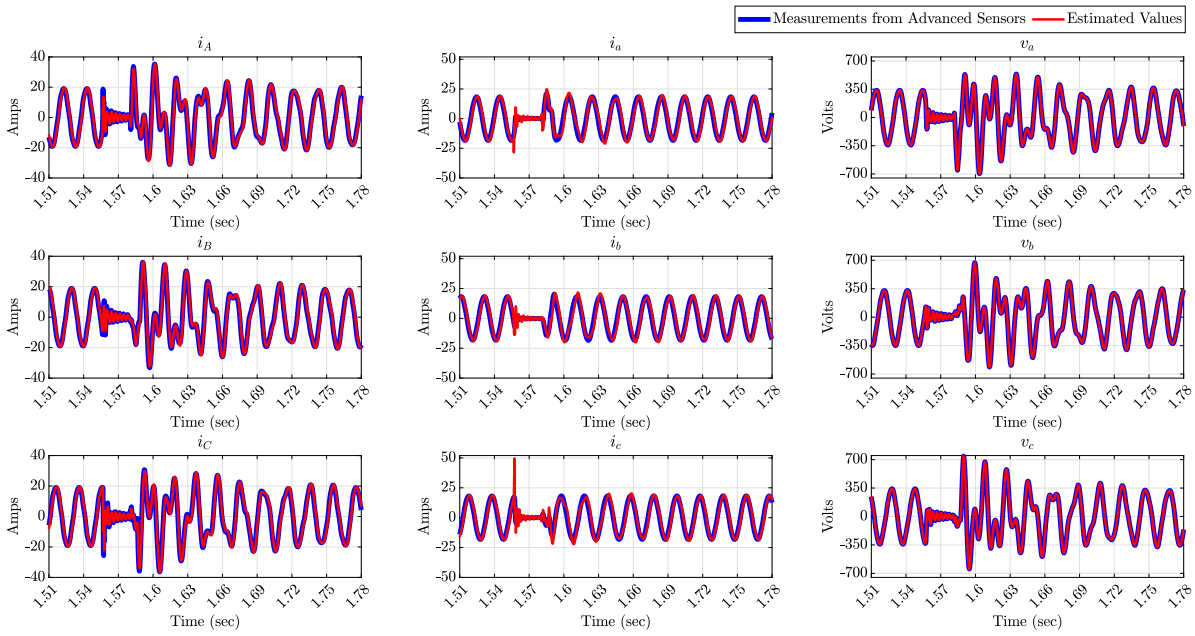

Fig. 17. Validation results for an external fault in terms of measured and estimated values of the sending end currents (i_A, i_B, i_C), receiving end currents (i_a, i_b, i_c), and receiving end voltages (v_a, v_b, v_c).

The origination of transients could be due to the radial structure of the transmission line setup which means the fault current is fed from one end only and hence whenever the fault occurs in any π-section its impact could be seen in the other π-sections. Also, the capacitive line charging currents could lead to the origination of transients. Despite the transients, the estimated values are in concurrency with the measured values. However, there is a sharp spike in the objective function when the fault starts but soon after (within 5 ms) the objective function comes below the threshold value. Since the spike in the objective function is very impulsive and does not meet the criteria for lowering the confidence level i.e., remains above the threshold value for more than 40 samples, thus the confidence level remains high during this condition and hence the trip signal is not generated (which is desired). The results from this case study imply that DSEBPS clearly discriminates against the external fault and thus does not generate a trip signal.

4.7. Load change conditions

Load change is a frequent operation in power systems that might require changes in the protection settings (for example when load current contributes significantly to the fault current like in large induction motors) and failing to do so could lead to maloperation. In this case study, DSEBPS is validated for a case where a load change (in the form of load increment) occurs. The type of load employed in this case study is purely resistive. The initial load in the studied system is 0 kW, while it is increased up to 18 kW in four steps, each of 4.5 kW. The objective function corresponding to these load changes is obtained continuously and plotted in Fig. 19. It can be seen from Fig. 19 that as the first load change occurs (i.e., from 0 to 4.5 kW) at around 0.25 s, the objective function increases and settles at a new higher value (approximately 1e4). Again, as the load increases further (i.e., from 4.5 to 9 kW) at around 1 s, the objective function further increases and settles at a new higher value (approximately 3e4). Similar changes could be seen for the further increments i.e., from 9 to 13.5 kW and 13.5 to 18 kW. The result from the case study suggests that the change in the loading conditions has an impact on the objective function and subsequently the threshold value is required to be changed for achieving the correct operation.

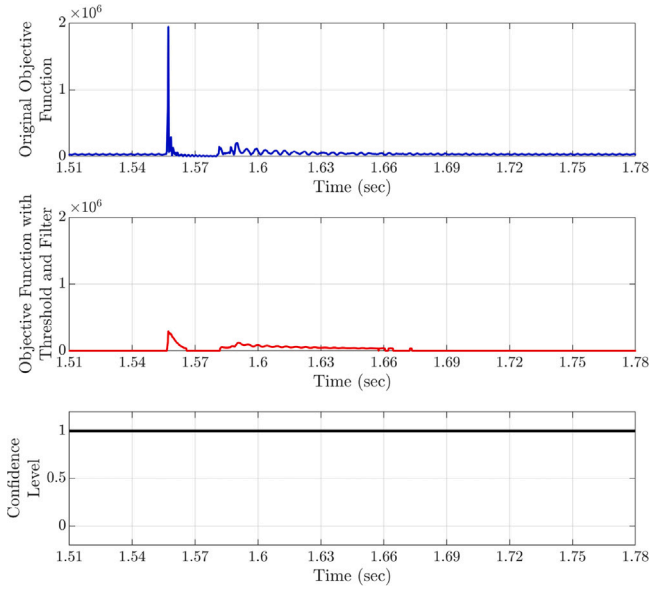

Fig. 18. Validation results for an external fault in terms of objective function and confidence level.

4.8. Lessons learned from experimental validation of DSEBPS

This subsection presents the lessons learned from results obtained with the experimental validation of DSEBPS.

- In the case of a high impedance fault, the overshoot in the objective function during the fault conditions is lower compared to the fault with a low or zero fault impedance path. It is due to the fact that during a high impedance fault, the fault currents do not shoot to a high value, unlike the fault with a zero fault impedance path, which results in a reduced mismatch between the measured and estimated values and hence reduced overshoot

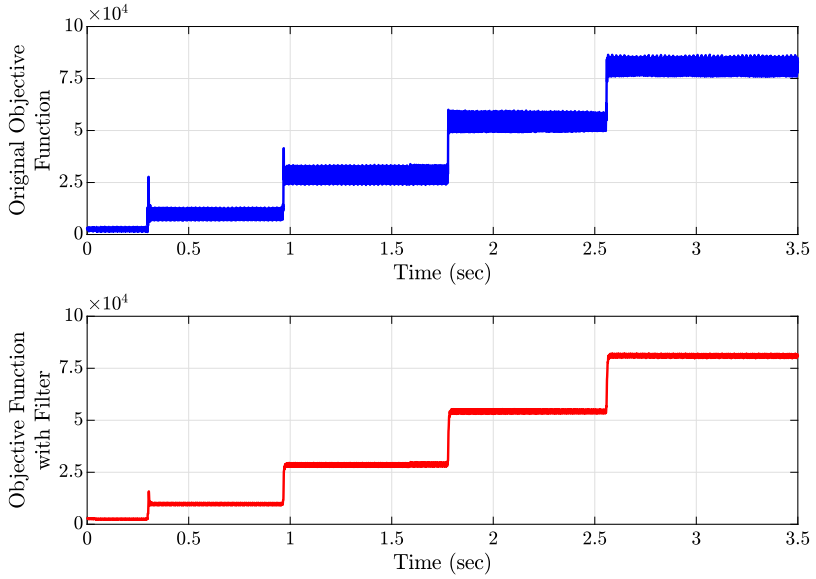

Fig. 19. Validation results for a load change in terms of the objective function and confidence level.

in the objective function. This observation provides motivation to explore further the limit of the fault impedance path until which the high impedance faults could be detected. The physical limitations of the experimental setup are a barrier to determining this limit.

- Under the load change conditions, the steady-state values of the objective function vary with the variations in load. From the case study presented in this paper, the general observation is that the increase in loading leads to an increase in the steady state value of the objective function. This observation signifies the direct connection of the objective function with the loading conditions and suggests the objective function threshold value could be adaptive to the load changes. The application of machine learning techniques could be one of the potential solutions to determine the threshold value in real-time.
- In a case study with fault current fed from both ends, the objective function has higher values compared to the fault fed from one end, while the overshoot in the objective function values during the fault conditions is smaller compared to the fault fed from one end and also shows an oscillatory nature. Due to the smaller overshoot in the objective function, reduced leverage is available for distinguishing the normal and fault conditions. The threshold value for the objective function is required to be changed based on the values obtained during normal operating conditions. These changes mainly occur due to the change in the network configuration by the addition of a synchronous generator.

5. Estimation error

Estimation error is one of the important indicators for evaluating the performance and accuracy of the SE algorithm. In order to evaluate the estimation error for the WLS SE algorithm used in this work, the following formulation is used:

Estimation error = Measured value – Estimated value

To obtain the estimation error distribution, the estimation error is calculated for 10 000 samples (collected during the normal operating conditions), and thereafter a histogram of the obtained errors is plotted along with the normal distribution fit as shown in Fig. 20. The function *histfit* in MATLAB R2021a is used for this purpose. The number of bins used in these plots is 30. Since the estimation error could vary based on the type of measurements (i.e., voltages and currents), therefore the estimation error is plotted separately for sending end current, receiving end current, and receiving end voltage, however, due to space limitations, these are plotted only for phase-A.

It can be seen from Fig. 20 that the standard deviation of the estimation error for the sending end current (i_A) ranges approximately between −5 and 5, for receiving end current (i_a) between −7 and 7, and for receiving end voltage (v_a) between −0.25 and 0.25. However, the mean of the estimation errors in all the cases remains close to zero. The main inference from the plots is that the estimation error is much lower in the case of receiving end voltage compared to sending end current and receiving end current, while the estimation error is within the same range in the case of sending end current and receiving end current.

6. Fault detection time

The fault detection time is an important criterion to evaluate the performance of a protection scheme. For good performance, the scheme should be able to detect the fault within the standard fault detection time. Distance protection, one of the most widely employed protection

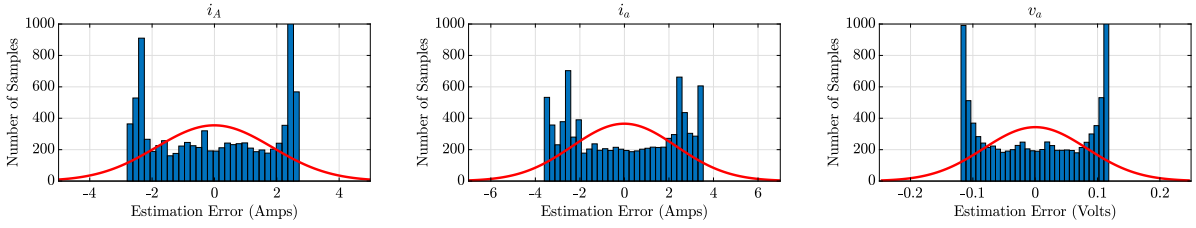

Fig. 20. Histogram plot with distribution fit for the estimation error in sending end current (i_A), receiving end current (i_a), and receiving end voltage (v_a) of phase-A.

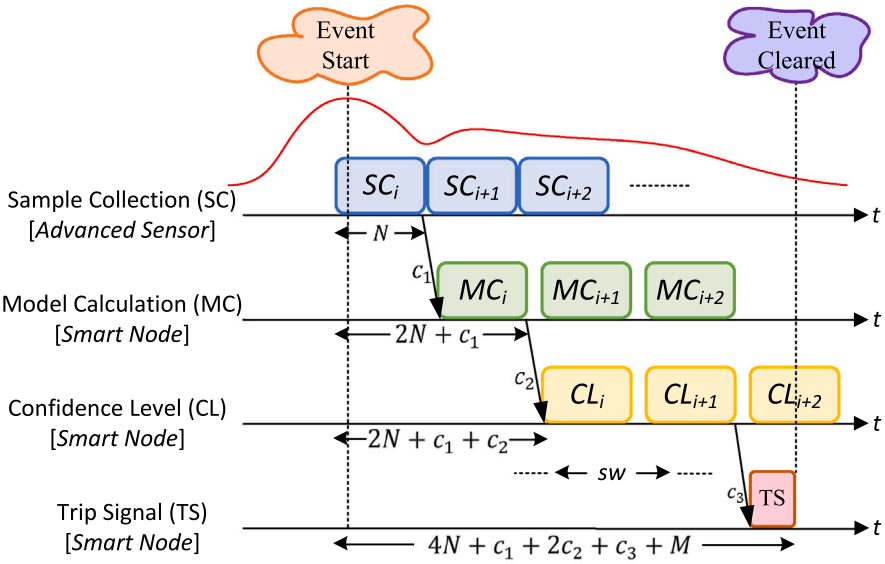

Fig. 21. Timing diagram showing different steps such as sample collection, model calculation, confidence level, and trip signal generation involved in DSEBPS.

schemes in transmission systems, takes around 1 to 2 cycles (20 to 40 ms in a 50 Hz system) for fault detection depending on how close to the relay the fault has occurred. Therefore, a performance analysis is done with regard to the fault detection time of DSEBPS. From the implementation diagram of DSEBPS as presented in Fig. 2, the main components of the fault detection time include sample collection time, communication time for a sample block to reach smart node (c_1), model calculation time, communication time from model calculation step to confidence level step (c_2), confidence level calculation time, communication time from confidence level step to trip signal step (c_3), and trip signal generation time. To avoid missing any signal events, sample block streaming and processing calculations are done continuously. Further, processing time and communication delays must be less than the time required to capture a sample block in order to ensure processing in real-time. A block size of 40 samples is chosen in this work so that it is large enough to contain the fault frequency information and minimize the noise effects. Although the samples are sent in blocks, they are processed on a per-sample basis and keep the same timestamp. Therefore, any processing delay is not visible in the result plots as presented in Section 4.

The timing diagram showing different steps from the instant when the event started until the event is cleared is presented in Fig. 21. The first step includes the sample collection (SC) step and requires time which is $N(= 40 \times 250 \ \mu s = 10$ ms). The model calculation (MC) step is triggered by the reception of the sample block and requires time which is N to reach the confidence level calculation step. The confidence level (CL) step operates in a sliding window (sw) with 40 samples which slide over the results of the MC step. The logic of the trip signal is designed using the confidence level signal which is based on the consistency of the objective function. For increased reliability of DSEBPS, the confidence level goes low if the objective function remains above the threshold for forty consecutive samples. It implies that the worst-case delay for the CL step could stretch over two sample blocks and hence two sample blocks are required for accurate calculation of the confidence level. Thus, the confidence level step requires time which is $2N$ to reach the trip signal decision. Once the CL determination is done a trip signal is generated and requires time which is M and sent to the circuit breakers' for clearing the fault. The communication time required for a sample block to reach from SC step to MC step is c_1, MC step to CL step is c_2, and CL step to TS step is c_3. Thus, the fault detection time (in the worst case) using DSEBPS comes out as $4N + c_1 + 2c_2 + c_3 + M$. In practice, the communication delays $c_1, c_2,$ and c_3 are generally very small as compared to processing delays and thus neglected. Further, the time for the trip signal generation (M) is considered 2.5 ms, and the circuit breaker operating time (mechanical device) is widely considered to be 2 cycles (40 ms in the case of a 50 Hz system). Thus, the fault detection time (in the worst case) is 42.5 ms, while the fault clearing time (in the worst case) is 82.5 ms as tested in the lab.

7. Conclusion

In this paper, a transmission line protection scheme using dynamic state estimation has been validated in a laboratory environment and proven to work satisfactorily under different fault types and conditions. Further, adequate performance is achieved in terms of selectivity and time during the experimental validation of the scheme. During normal operating conditions and external faults, the trip signal is not generated (avoiding unwanted tripping), while the trip signal is successfully generated during unbalanced faults, fault with inductive load conditions, high impedance fault, fault current fed from both ends, and hidden failure. The key outcomes from the validation demonstrate the advantages of the scheme such as avoidance of complex relay settings and coordination, which could substantially reduce the mis-operations caused by incorrect relay settings. Future works could involve advancements in the DSE method to reduce processing time, reduce the redundancy ratio and dependency on communication infrastructure. Extending the experimental validation of DSEBPS to other power system components such as transformers, alternators, inverters, etc, could also be explored. The validation of each of these components could lay the foundation for the development, implementation, and validation of a dynamic state estimation-based centralized protection scheme for a power system.

CRediT authorship contribution statement

Ankur Srivastava: Conceptualization, Methodology, Software, Validation, Formal analysis, Investigation, Writing – original draft, Writing – review & editing, Visualization. **Le Anh Tuan:** Conceptualization, Methodology, Validation, Formal analysis, Resources, Writing – review & editing, Supervision, Project administration, Funding acquisition. **David Steen:** Conceptualization, Methodology, Formal analysis, Resources, Writing – review & editing, Supervision, Project administration, Funding acquisition. **Ola Carlson:** Formal analysis, Writing – review & editing, Supervision, Project administration. **Omar Mansour:**

Methodology, Software, Validation, Resources, Writing – review & editing. **Dennis Bijwaard:** Methodology, Software, Validation, Resources, Writing – review & editing.

Declaration of competing interest

The authors declare that they have no known competing financial interests or personal relationships that could have appeared to influence the work reported in this paper.

Data availability

The research data used in this work is presented in the paper.

Acknowledgments

The work presented in this paper is financially supported by the following projects: (i) UNITED-GRID - received funding from the European Community's Horizon 2020 Framework Programme under grant agreement no. 773717; (ii) FLEXI-GRID - received funding from the European Community's Horizon 2020 Framework Programme under grant agreement no. 864048.

References

[1] NERC. Analysis of system protection misoperations. 2015, [Online] Available: https://www.nerc.com/pa/RAPA/PA/Performance%20Analysis%20DL/2015_Analysis_of_System_Protection_Misoperations_Final.pdf.
[2] Srivastava A, Mohanty R, Ghazvini MAF, Tuan LA, Steen D, Carlson O. A review on challenges and solutions in microgrid protection. In: Proc. IEEE Madrid Powertech. 2021, p. 1–6.
[3] Meliopoulos APS, et al. Dynamic state estimation-based protection: Status and promise. IEEE Trans Power Deliv 2016;32(1):320–30.
[4] Liu Y, Meliopoulos APS, et al. Dynamic state estimation based protection on series compensated transmission lines. IEEE Trans Power Deliv 2016;32(5):2199–209.
[5] Xu Z, Du Z, Ran L, Wu Y, Yang Q, He J. A current differential relay for a 1000-kV UHV transmission line. IEEE Trans Power Deliv 2007;22(3):1392–9.
[6] Telukunta V, et al. Protection challenges under bulk penetration of renewable energy resources in power systems: A review. CSEE J Power Energy Syst 2017;3(4):365–79.
[7] Zhao J, et al. Power system dynamic state estimation: Motivations, definitions, methodologies, and future work. IEEE Trans Power Syst 2019;34(4):3188–98.
[8] Liu Y, Singh AK, Zhao J, et al. Dynamic state estimation for power system control and protection IEEE task force on power system dynamic state and parameter estimation. IEEE Trans Power Syst 2021;36(6):5909–21.
[9] Meliopoulos APS, et al. Setting-less protection: Feasibility study. In: Proc. 46th Hawaii International Conference on System Sciences. 2013, p. 2345–53.
[10] Xie J, Meliopoulos APS, Xie B. Transmission line fault classification based on dynamic state estimation and support vector machine. In: Proc. IEEE NAPS. 2018, p. 1–5.
[11] Liu K, Meliopoulos APS, et al. Dynamic state estimation-based protection of distribution systems with high penetration of DERs. In: Proc. IEEE PES General Meeting. 2020, p. 1–5.
[12] Albinali HF, Meliopoulos APS. Resilient protection system through centralized substation protection. IEEE Trans Power Deliv 2018;33(3):1418–27.
[13] Rimorov D, Brissette Y, Kamwa I, Joós G. Synchrophasor-based state estimation for microgrid protection. In: Proc. IEEE PES General Meeting. 2018, p. 1–5.
[14] Cui Y, et al. Dynamic state estimation assisted posturing for generator out-of-step protection. In: Proc. IEEE PES General Meeting. 2016, p. 1–5.
[15] Wang B, et al. Transmission line fault location in MMC-HVDC grids based on dynamic state estimation and gradient descent. IEEE Trans Power Deliv 2020;36(3):1714–25.
[16] Shalini, et al. Enhancing performance of wide-area back-up protection scheme using PMU assisted dynamic state estimator. IEEE Trans Smart Grid 2018;10(5):5066–74.
[17] Srivastava A, Tuan LA, Steen D, Carlson O, Mansour O, Bijwaard D. Transmission line protection using dynamic state estimation and advanced sensors: Experimental validation. IEEE Trans Power Deliv 2023;38(1):162–76.
[18] Meliopoulos AP, Cokkinides GJ, Stefopoulos GK. Quadratic integration method. In: Proc. Citeseer International Power System Transients Conference. 2005, p. 19–23.
[19] Lee YH. A comprehensive protection scheme for distribution systems (Ph.D. thesis), Atlanta, USA: Georgia Institute of Technology; 2014.
[20] Srivastava A. Operation, monitoring, and protection of future power systems: advanced congestion forecast and dynamic state estimation applications (Ph.D. thesis), Sweden: Chalmers University of Technology; 2022.
[21] Srivastava A, Chakrabarti S, Soares J, Singh SN. An optimization-based topology error detection method for power system state estimation. Electr Power Syst Res 2022;209:107914.
[22] Chakrabarti S, Kyriakides E, Valverde G, Terzija V. State estimation including synchronized measurements. In: Proc. IEEE Bucharest Powertech. 2009, p. 1–5.
[23] Smart state technology, The Netherlands. 2022, [Online] Available: https://www.smartstatetechnology.nl/.